

Q-Flow: Generative Modeling for Differential Equations of Open Quantum Dynamics with Normalizing Flows

Owen Dugan¹ Peter Y. Lu² Rumen Dangovski³ Di Luo^{4,5,6} Marin Soljačić¹

Abstract

Studying the dynamics of open quantum systems holds the potential to enable breakthroughs both in fundamental physics and applications to quantum engineering and quantum computation. Due to the high-dimensional nature of the problem, customized deep generative neural networks have been instrumental in modeling the high-dimensional density matrix ρ , which is the key description for the dynamics of such systems. However, the complex-valued nature and normalization constraints of ρ , as well as its complicated dynamics, prohibit a seamless connection between open quantum systems and the recent advances in deep generative modeling. Here we lift that limitation by utilizing a reformulation of open quantum system dynamics to a partial differential equation (PDE) for a corresponding probability distribution Q , the Husimi Q function. Thus, we model the Q function seamlessly with *off-the-shelf* deep generative models such as normalizing flows. Additionally, we develop novel methods for learning normalizing flow evolution governed by high-dimensional PDEs, based on the Euler method and the application of the time-dependent variational principle. We name the resulting approach *Q-Flow* and demonstrate the scalability and efficiency of Q-Flow on open quantum system simulations, including the dissipative harmonic oscillator and the dissipative bosonic model. Q-Flow is superior to conventional PDE solvers and state-of-the-art physics-informed neural network solvers, especially in high-dimensional systems.

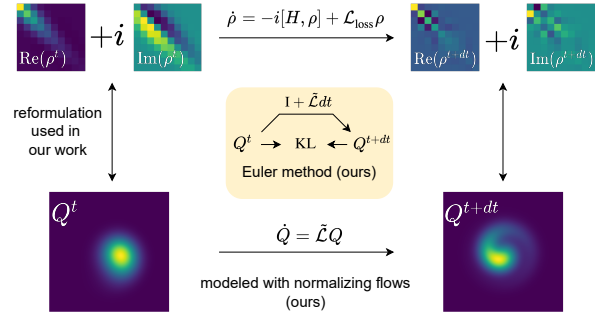


Figure 1. Q-Flow. Reformulated density matrix dynamics in continuous systems to a PDE for probability distributions. Off-the-shelf normalizing flows, and our Euler-KL method are used to solve such PDEs.

1. Introduction

Understanding the dynamics of open quantum systems is a necessary step towards advances in fundamental physics and high-impact scientific applications such as quantum engineering and quantum computation (Verstraete et al., 2009; Barreiro et al., 2011). The dynamics of such systems depend on the *density matrix* ρ , which describes all the information of a quantum many-body system. The density matrix is an exponentially scaling object in the double Hilbert space whose complexity grows as N^{2k} for N local degrees of freedom and k sites. Thus, solving for ρ suffers from the curse of dimensionality.

Pioneering work on representing ρ in a compact form as a customized deep generative neural network has shown great promise in advancing the frontier of understanding high-dimensional quantum systems (Vicentini et al., 2019; Yoshioka & Hamazaki, 2019; Hartmann & Carleo, 2019; Nagy & Savona, 2019). However, a number of computational challenges remain when solving for ρ , which motivates the development of novel machine learning methods. Notable challenges are:

1. The density matrix ρ is *complex-valued* and has the constraint $\text{tr}[\rho] = 1$. That makes it non-trivial to model with standard deep generative models, which are real-valued.

¹Department of Physics, Massachusetts Institute of Technology
²University of Chicago ³MIT EECS ⁴NSF AI Institute for Artificial Intelligence and Fundamental Interactions ⁵Center for Theoretical Physics, Massachusetts Institute of Technology ⁶Department of Physics, Harvard University. Correspondence to: Di Luo <diluo@mit.edu>.

2. The partial differential equation (PDE) that governs the dynamics of ρ models complicated interactions, which hampers the application of standard machine learning PDE solvers.
3. Previous efforts on modeling ρ with neural networks are restricted to discrete spin systems, and it is unclear how to model ρ in continuous space or bosonic systems.

The state-of-the-art literature has addressed Challenge 1 by developing customized neural architectures for ρ in spin systems with discrete degrees of freedom only (Vicentini et al., 2019; Yoshioka & Hamazaki, 2019; Hartmann & Carleo, 2019; Nagy & Savona, 2019; Luo et al., 2022b; Reh et al., 2021). Challenge 2 has been attempted by exploring physics-inspired training objectives, such as Physics-informed neural networks (PINNs) (Raissi, 2018; Raissi et al., 2019). PINNs have shown promise in low-dimensional systems but it is not clear how they can scale to high-dimensional PDEs. Furthermore, the existing literature has not addressed Challenge 3 and missed an opportunity to establish a *direct* connection between progress in modeling open quantum dynamics and novel deep generative models for standard machine learning benchmarks. Such a connection would drive progress in both machine learning applications for open quantum dynamics and deep generative modeling.

In this paper, we address Challenges 1-3 by establishing a bridge between open quantum systems and continuous-variable generative modeling.

Firstly, we reformulate the problem by replacing the density matrix ρ with an alternative representation, the Husimi Q function Q (Carmichael, 1999b), which can be practically considered as a probability distribution. Thus, we enable the use of *off-the-shelf* generative neural networks to model Q . Because variational Monte Carlo methods for quantum systems require access to both easy sampling and probability density values, we use *normalizing flows* (Dinh et al., 2014; Rezende & Mohamed, 2015) as our generative model.

Secondly, we develop novel methods for training normalizing flows that obey complicated high-dimensional PDEs, which are an excellent fit for approximating Q . We propose a training method, the stochastic *Euler-KL* method, which is based on the forward discretization of the differential equation for Q and the Kullback-Liebert matching of probability distributions. Our normalizing flows approach can also be equipped with the Time-Dependent Variational Principle (TDVP) method (McMillan, 1965), which can be derived from the Euler method and can be thought of as an analog of the natural gradient method (Amari, 1996; 1998).

We name our contributions *Q-Flow* (see Figure 1). Q-Flow is a new approach to solving open quantum systems based on off-the-shelf normalizing flows and the Euler/ TDVP

methods for evolving such flows in complicated PDEs. We demonstrate that Q-Flow is scalable and efficient for simulating various open quantum systems. Our contributions can be summarized as follows:

- New generative modeling approach for open quantum dynamics with continuous degrees of freedom based on the Husimi Q function, which allows for using normalizing flows off-the-shelf.
- New methods for solving open quantum dynamics PDEs using normalizing flows with stochastic Euler-KL method and TDVP.
- Demonstration of the scalability and efficiency of our methods on simulations of dissipative harmonic oscillator and dissipative bosonic models by surpassing conventional PDE solvers and state-of-the-art machine learning PDE solvers, physics-informed neural networks (PINN).

Importantly, with Q-Flow, the difficulty in simulating quantum dynamics is no longer the dimension of the simulation but instead the complexity of the Q function and its evolution, which opens a new avenue for research.

2. Related Work

2.1. Neural Network Quantum States

Neural network quantum states are generative neural network architectures—including restricted Boltzmann machines (Carleo & Troyer, 2017), autoregressive models (Sharir et al., 2020; Luo et al., 2022a; Chen et al., 2022; Luo et al., 2021), and determinant neural network models (Pfau et al., 2020; Hermann et al., 2020; Luo & Clark, 2019)—that have been adapted to represent quantum wave functions or density matrices (in the case of open quantum systems) rather than probability distributions. They are optimized using variational quantum Monte Carlo methods and have primarily been applied to model discrete spin systems (Carleo & Troyer, 2017; Sharir et al., 2020; Luo et al., 2022a) as well as tackle the continuous many-body wave function in quantum chemistry (Pfau et al., 2020; Hermann et al., 2020), condensed matter (Pescia et al., 2022; Medvidović & Sels, 2022) and quantum field theories (Luo et al., 2022c; Martyn et al., 2022).

In contrast with prior deep learning-based approaches that directly model the wave function or density matrix, our work focuses on the Q function representation of the quantum state—a continuous quasiprobability distribution (Carmichael, 1999b) that can be modeled using an appropriate generative model, e.g. normalizing flows.

2.2. Partial Differential Equation (PDE) Solvers

To model the dynamics of an open quantum system using the Q function formulation, we are required to solve a high-dimensional PDE. By parameterizing the Q function using a normalizing flow, our approach can efficiently solve this PDE. For comparison, we benchmark our work against alternative PDE solvers.

Traditional PDE solvers struggle to handle high-dimensional PDEs due to the curse of dimensionality, where even storing the state of the system on a grid or mesh grows exponentially with the dimension of the problem. As a comparison, we use a simple pseudo-spectral method (Fornberg, 1998) as our traditional solver benchmark. While there are specialized methods for solving high-dimensional PDEs, they are often complex to set up and only apply to a few restricted classes of PDEs, e.g. parabolic PDEs (Weinan et al., 2021).

We also benchmark against physics informed neural networks (PINNs)—a promising deep learning-based variational approach for solving PDEs (Raissi, 2018; Raissi et al., 2019; Berg & Nyström, 2019). PINNs, however, have been shown to have limitations related to the difficulty of the variational optimization problem (Krishnapriyan et al., 2021) and, in their standard form, may also suffer from the curse of dimensionality.

3. Solving Open Quantum Dynamics with Q-Flow

In this work, we develop Q-Flow, an approach for solving open quantum dynamics based on flow-based models under the Q function partial differential equation formulation. The key contributions of our work are twofold. Firstly, we establish a general framework for solving open quantum dynamics learning through the flow-based model representation. Secondly, we develop optimization algorithms for solving high dimensional partial differential equations and apply them to PDEs for the Q function.

3.1. Open Quantum System

A generic Markovian open quantum system starts with the following form

$$\dot{\rho} = \mathcal{L}\rho = -i[H, \rho] + \mathcal{L}_{\text{loss}}\rho, \quad (1)$$

where ρ is the density matrix, H is the Hamiltonian, $\mathcal{L}_{\text{loss}}$ is the dissipative operator, and $[\cdot, \cdot]$ is the commutation operator between matrices, i.e. $[A, B] = AB - BA$.

In general, ρ is a complex-valued density matrix whose size grows exponentially with the number of particles. The density matrix ρ is a generalization of the wave function in the Schrödinger equation, which can be viewed as an ensemble

of wave functions. We note that Eq. 1 is a complex-valued high-dimensional differential equation, which is challenging to be solved in general.

In this work, we focus on bosonic open quantum dynamics with continuous degree of freedom, which arises in a variety of contexts (Cazalilla et al., 2011; Adesso et al., 2014). A bosonic particle, also known as a *boson*, is one kind of fundamental particle in quantum mechanics. A boson has continuous degrees of freedom, which could be more challenging to represent compared to discrete variable systems such as spin systems. In practice, one workaround is to truncate the infinite continuous degree of freedom to some large finite degree K . Regardless of the truncation effect, bosons at M Wells still live in an exponentially-large-dimensional Hilbert space of size M^K , which is intractable to simulations in general.

3.2. Q Function Formulation

The Husimi Q function (Carmichael, 1999a) provides an exact reformulation of Eq. 1 into a probabilistic differential equation:

$$\dot{Q} = \tilde{\mathcal{L}}Q \quad (2)$$

where Q is called the Husimi Q function and $\tilde{\mathcal{L}}$ is the corresponding operators transformed from the Hamiltonian operator H and the dissipative operator $\mathcal{L}_{\text{loss}}$.

Mathematically, the Q function of one particle is related to density matrix ρ through $Q(\alpha, \alpha^*) = \frac{1}{\pi} \langle \alpha | \rho | \alpha \rangle$, where $\alpha = x + iy$ is a complex number, and $|\alpha\rangle$ is known as the coherent state (see Appendix A.1 for more details). $Q(\alpha, \alpha^*) \geq 0$ for any α and $\int Q = 1$, so Q can be interpreted as a probability distribution in practice.

To efficiently apply the Q function formalism, we must be able to easily convert between the ρ and Q functions and obtain $\tilde{\mathcal{L}}$. We supplement the key conversion formulas and the corresponding proofs in Appendix A.

3.3. Q-Flow representation: Flow-based Generative Models of Q function

One important feature of our work is to represent the Q function with off-the-shelf flow-based generative models. Thus, our work is distinguished from the previous works (Vicentini et al., 2019; Yoshioka & Hamazaki, 2019; Hartmann & Carleo, 2019; Nagy & Savona, 2019) that represent the high dimensional complex-valued density matrix using customized neural networks. There are several advantages of our approach. Firstly, we do not need to work with complex-valued functions, which could be complicated by the sign structure problem (Westerhout et al., 2020). Secondly, Q-Flow is natural for systems with continuous degrees of free-

dom. Thirdly, Q-Flow allows normalized probability modeling with exact sampling, which is important for solving high dimensional probabilistic PDEs with the stochastic Euler method.

Normalizing Flows. Normalizing flows are generative models for continuous probability distributions that provide both normalized probabilities and exact sampling—making them ideal for modeling the continuous Q function in our approach. Normalizing flows transform a simple initial density p_X (often a unit normal distribution) to a target density p_Y (i.e. the distribution that we want to model) via a sequence of invertible transformations (Dinh et al., 2014; Rezende & Mohamed, 2015). The invertible transformations are usually parameterized by an invertible neural network architecture $y = f_\theta(x)$ with $x \sim p_X$ and $y \sim p_Y$. The target probability density is then given by

$$p_Y(y) = p_X(f_\theta^{-1}(y)) \left| \frac{f_\theta^{-1}(y)}{\partial y} \right|.$$

Many choices of f_θ are available, including affine coupling layers (RealNVP) (Dinh et al., 2017), continuous normalizing flows (CNF) (Grathwohl et al., 2019), and convex potential flows (CP-Flow) (Huang et al., 2021). While RealNVP is the simplest to implement, affine coupling layers are less expressive than CNFs or CP-Flows, which are provably universal density estimators (Huang et al., 2021). In addition, because of Equation 10, we would like our flow to be infinitely differentiable which are satisfied by the above flow architectures.

Theorem 3.1. *For a Q function from a given density matrix ρ , there exists a universal approximation with a Q-Flow representation.*

Proof. For any given density matrix ρ , there is a corresponding Q_ρ which satisfies $Q_\rho \geq 0$ and $\int Q_\rho = 1$. Here, one can view Q_ρ practically. Since it has been shown that normalizing flows are universal approximations of probability distributions (Huang et al., 2021), there exists a Q-Flow representation Q_f such that Q_f can be arbitrarily close to Q_ρ . \square

Theorem 3.2. *For any local observable expected value to be computed with respect to ρ , there exists a Q-Flow representation which can compute the observable efficiently.*

Proof. Consider the corresponding Q function Q_ρ of ρ . Consider a local observable in the form of $O = a^m a^{\dagger n} + a^n a^{\dagger m}$. WLOG, we can consider $O = a^m a^{\dagger n}$, the reasoning for the remaining part is analogous. The expectation is $\langle O \rangle_\rho = \text{tr}(\rho a^m a^{\dagger n})$. Eq. A.5 in the Appendix shows that it can be equivalently computed by $\int (q + ip)^m (q - ip)^n Q_\rho(p, q) dp dq$, which is a certain polynomial moment of the Q function. Since normalizing flows are a universal approximators, there exists a Q-Flow representation Q_f

Algorithm 1 Stochastic Euler-KL Method

Input: normalizing flow models for Q_θ^{t+dt} and Q^t , total time T , time step dt , n_{iter} , optimizer Adam.
Output: Optimal parameters θ^* at time step $t + dt$
Initialization: Random $\theta(t_0)$
for j in range(T/dt) **do**
 for $i = 0$ to n_{iter} **do**
 update θ using Eq. 5 and optimizer Adam
 end for
 $Q^t \leftarrow Q_\theta^{t+dt}$
end for

that can be arbitrarily close to Q_ρ , which implies that $\langle Q \rangle_f$ can be arbitrarily close to $\langle Q \rangle_\rho$. Even though computing $\langle Q \rangle_f = \sum_{p,q \sim Q_f} (q + ip)^m (q - ip)^n$ has stochastic fluctuations, the exact sampling nature of the flow-based model can suppress the statistical error, which will decay with the increasing sample size N_s as $\frac{1}{\sqrt{N_s}}$ due to the Central Limit Theorem. \square

3.4. Q-Flow Optimization: Stochastic Euler-KL Method

In the previous section, we discuss the representation of the Q function with flow-based models. To solve the real-time dynamics given by Eq. 2, we further develop the high dimensional stochastic Euler-KL method.

The algorithm represents the Q function at time t with a flow-based model and iteratively updates the representation at the next time $t+dt$ based on the Euler method. Concretely, it requires two copies of flow-based models for Q^{t+dt} and Q^t . Based on the first-order Euler method with time step dt , Eq. 2 yields

$$Q^{t+dt} = Q^t + \tilde{\mathcal{L}} Q^t dt = (I + \tilde{\mathcal{L}} dt) Q^t \equiv Q_{\mathcal{L}}^t. \quad (3)$$

Notice that Q^{t+dt} represents the Q function that we obtain in the next time step. At each learning step, we fix Q^t and optimize the parameters θ in Q_θ^{t+dt} to match the above relation. Hence, we also denote Q^{t+dt} by Q_θ^{t+dt} . It facilitates us to define the following loss function through KL divergence.

$$KL(Q_\theta^{t+dt} || Q_{\mathcal{L}}^t) = \int Q_\theta^{t+dt} \ln \frac{Q_\theta^{t+dt}}{Q_{\mathcal{L}}^t} \quad (4)$$

The gradient of Eq. 4 can be derived with a control variance technique as follows (see Appendix for a derivation):

$$\frac{1}{N} \sum_{x \sim Q_\theta^{t+dt}} \left[\ln \frac{Q_\theta^{t+dt}(x)}{Q_{\mathcal{L}}^t(x)} - b \right] \nabla_\theta \ln Q_\theta^{t+dt}(x) \quad (5)$$

where $b = \frac{1}{N} \sum_{x \sim Q_{\theta}^{t+dt}} \ln \frac{Q_{\theta}^{t+dt}(x)}{Q_{\mathcal{L}}(x)}$ is the baseline for control variance.

The stochastic Euler-KL method is summarized in Algorithm. 1.

Theorem 3.3. *The global error $\epsilon(t_n)$ of the n -step stochastic Euler method is bounded by $|\epsilon_E(t_n)| + |\epsilon_{NN}(t_n)|$, where $\epsilon_E(t_n)$ is the global error of the exact Euler method and $\epsilon_{NN}(t_n) = -P^{-1} \sum_{i=0}^n P^i r^{n+1-i}$ with $P = I + \tilde{\mathcal{L}}dt$ and r^i being the i -th step stochastic Euler optimization error with neural network representation of the Q-Flow.*

Proof. $\epsilon(t_n) = Q^{t_n} - Q_{NN}^{t_n} = (Q^{t_n} - Q_E^{t_n}) + (Q_E^{t_n} - Q_{NN}^{t_n}) \equiv \epsilon_E(t_n) + \epsilon_{NN}(t_n)$, where $Q_E^{t_n}$ and $Q_{NN}^{t_n}$ are the Q function from the exact Euler method and the neural network Q-Flow at time step t_n . By the triangular inequality, $|\epsilon(t_n)| \leq |\epsilon_E(t_n)| + |\epsilon_{NN}(t_n)|$. Since the Euler method is a first order method, it has global error with order $O(dt)$ where dt the time step.

Denote the optimization error of Eq. 4 at time step t_{n+1} as r^{n+1} , such that $Q_{NN}^{t_{n+1}} - PQ_{NN}^{t_n} = r^{n+1}$. It follows that $Q_E^{t_{n+1}} - \epsilon_{NN}(t_{n+1}) - P(Q_E^{t_n} - \epsilon_{NN}(t_n)) = r^{n+1}$, which implies that $\epsilon_{NN}(t_{n+1}) = P\epsilon_{NN}(t_n) - r^{n+1}$ due to the cancellation of $Q_E^{t_{n+1}} - PQ_E^{t_n}$ from the exact Euler method. By induction, we have $\epsilon_{NN}(t_n) = -P^{-1} \sum_{i=0}^n P^i r^{n+1-i}$. \square

Time Dependent Variational Principle (TDVP). Instead of taking gradient with respect to the KL divergence as Eq. 5 shows, Reh & Gärtner (2022) demonstrate that the minimization of Eq. 4 is equivalent to the time dependent variational principle, which provides a nonlinear differential equation on the parameter space θ as $S_{kk'} \dot{\theta}_{k'} = F_k$, where $S_{kk'} = \mathbb{E}[(\partial_{\theta_k} \ln Q)(\partial_{\theta_{k'}} \ln Q)]$ is the Fisher information matrix, and $F_k = \mathbb{E}[(\partial_{\theta_k} \ln Q)(\partial_t \ln Q)]$.

Reh & Gärtner (2022) apply TDVP only to solving classical PDEs. Under our Q-Flow approach, we can also apply TDVP to simulate open quantum dynamics.

Complexity Analysis. Even though the stochastic Euler-KL method and the TDVP method are equivalent mathematically, they share different algorithmic complexity. TDVP requires to solve the nonlinear different equation, which needs to invert the Fisher information matrix $S_{kk'}$. Besides potential instability, this procedure has complexity scaling as $O(N^3)$ for explicit inversion or $O(N^2)$ at least with the conjugate gradient approach, where N is the number of parameters. It may limit its application for parameters beyond the orders of ten thousands. Meanwhile, the stochastic Euler method only requires first order optimization based on Eq. 5, the main cost of which comes from the number of optimization steps in each dt .

Table 1. The loss $L_1[Q_{\text{sim}}, Q_{\text{exact}}]$ for each simulation method over time (in a unit inversely proportional to the unit of γ_j). For each row, we mark the best result in bold. PS data for 20-Well does not exist because PS does not scale to high-dimensional problems.

1-Well				
Time	Q-Flow(Euler) (ours)	Q-Flow(TDVP) (ours)	PINN	PS
3	$2.08 \cdot 10^{-3}$	$5.11 \cdot 10^{-3}$	$1.79 \cdot 10^{-1}$	$1.45 \cdot 10^{-4}$
6	$5.10 \cdot 10^{-4}$	$1.17 \cdot 10^{-3}$	$1.84 \cdot 10^{-1}$	$1.37 \cdot 10^{-4}$
9	$1.01 \cdot 10^{-4}$	$2.16 \cdot 10^{-4}$	$1.91 \cdot 10^{-1}$	$1.43 \cdot 10^{-4}$
12	$1.68 \cdot 10^{-5}$	$3.58 \cdot 10^{-5}$	$1.91 \cdot 10^{-1}$	$1.50 \cdot 10^{-4}$
15	$1.58 \cdot 10^{-5}$	$5.55 \cdot 10^{-6}$	$1.98 \cdot 10^{-1}$	$6.29 \cdot 10^{-5}$
2-Well				
3	$3.91 \cdot 10^{-3}$	$1.23 \cdot 10^{-2}$	$2.10 \cdot 10^{-1}$	$4.93 \cdot 10^{-1}$
6	$1.91 \cdot 10^{-3}$	$4.66 \cdot 10^{-3}$	1.00	$4.40 \cdot 10^{-1}$
9	$7.59 \cdot 10^{-4}$	$1.77 \cdot 10^{-3}$	1.00	$4.91 \cdot 10^{-1}$
12	$2.92 \cdot 10^{-4}$	$6.21 \cdot 10^{-4}$	1.00	$4.55 \cdot 10^{-1}$
15	$1.47 \cdot 10^{-4}$	$2.05 \cdot 10^{-4}$	1.00	$3.41 \cdot 10^{-1}$
20-Well				
3	$9.94 \cdot 10^{-2}$	$1.08 \cdot 10^{-1}$	$2.17 \cdot 10^{31}$	-
6	$3.29 \cdot 10^{-2}$	$4.10 \cdot 10^{-2}$	$2.38 \cdot 10^{30}$	-
9	$2.02 \cdot 10^{-2}$	$2.44 \cdot 10^{-2}$	$1.34 \cdot 10^{29}$	-
12	$1.46 \cdot 10^{-2}$	$1.68 \cdot 10^{-2}$	$1.46 \cdot 10^{28}$	-
15	$1.07 \cdot 10^{-2}$	$1.23 \cdot 10^{-2}$	$7.07 \cdot 10^{26}$	-

3.5. Q-Flow Initialization: Initial State Pretraining

Using a Q-Flow to simulate a quantum system requires initializing the flow to the correct starting Q function. For some simple initial states, we find that it is sufficient to simply make the initial state the prior for the flow and initialize the flow to the identity. However, we find that using more complex initial distributions as priors to a flow tends to hamper their ability to model a system’s evolution. In these cases, we instead use the standard Gaussian prior, but we use a two-step process to pretrain the flow to match the initial distribution Q_{init} .

First, we sample from the desired initial distribution using the Metropolis-Hastings Monte Carlo method and update the flow parameters to minimize the negative log likelihood $-\sum_{x \sim Q_{\text{init}}} \ln Q_{\theta}(x)$. This ensures that the model has some overlap with Q_{init} which helps the next step’s training algorithm converge more quickly.

Second, we sample from the flow and update the flow parameters to minimize the KL Loss, $KL(Q_{\text{init}}||Q_{\theta})$. We compute the gradient according to

$$\nabla_{\theta} KL \approx -\frac{1}{N} \sum_{x \sim Q_{\theta}} \frac{Q_{\text{init}}(x)}{Q_{\theta}(x)} \nabla_{\theta} \ln Q_{\theta}(x). \quad (6)$$

4. Experiments

For our experiments, we focus on two types of open quantum systems: dissipative harmonic oscillators and dissipative bosonic systems. We test on dissipative harmonic

oscillators because they have an analytic solution, which makes them useful for benchmarking high-dimensional PDE solvers beyond the limits of conventional solvers. We then test on dissipative bosonic systems because they are commonly studied and of practical use in physics.

In these experiments, we compare Euler and TDVP methods to PINNs and pseudo-spectral (PS) solvers. Although we do not develop the TDVP method, we propose a method to apply it to open bosonic quantum systems. As such, we sometimes describe the Euler and TDVP methods as “our methods.”

For our experiments, we use Affine Coupling Flows and Convex-Potential Flows for the Euler and TDVP methods. Affine Coupling Flows are fast but less expressive, so we use them for the dissipative harmonic oscillator experiments. On the other hand, Convex Potential Flows are slow but more expressive, so we use them for problems involving more complex Q functions.

To run our experiments, we use the Jax library (Bradbury et al., 2018) for Euler and TDVP methods. We make use of the `jax-flows` library. To implement the TDVP method, we make use of the NetKet library (Carleo et al., 2019; Vicentini et al., 2022) and its Stochastic Reconfiguration (Sorella, 1998; 2001) feature, which is mathematically equivalent to TDVP. For distributed training, NetKet uses the `mpi4jax` package (Häfner & Vicentini, 2021). For PINNs, we use the PINA library which is built on top of PyTorch (Paszke et al., 2019). Finally, for our pseudo-spectral methods we use Julia (Rackauckas & Nie, 2017).

4.1. Dissipative Harmonic Oscillator

Experimental Setup. The multi-well dissipative harmonic oscillator evolves according to Eq. 1 with Hamiltonian $H = \sum_j \omega_j a_j^\dagger a_j$ (Carmichael, 1999a) and loss term

$$\mathcal{L}_{\text{loss}}\rho = \sum_j \gamma_j \left[\frac{1}{2}(2a_j \rho a_j^\dagger - a_j^\dagger \rho - \rho a_j^\dagger a_j) + \bar{n}_j(a_j \rho a_j^\dagger + a_j^\dagger \rho a_j - a_j^\dagger a_j \rho - \rho a_j a_j^\dagger) \right]. \quad (7)$$

Here, j labels what we will call *Wells*.

To convert to the Q function formalism, we first define notation: For a Q function $Q(\alpha_1, \dots, \alpha_n)$, we define q and p such that $\alpha_j = q_j + ip_j$ and set $x = (\vec{q}, \vec{p})$. We use the notations $Q(\alpha_1, \dots, \alpha_n)$, $Q(\vec{q}, \vec{p})$, and $Q(x)$ interchangeably.

Now, converting to the Q function formalism with real in-

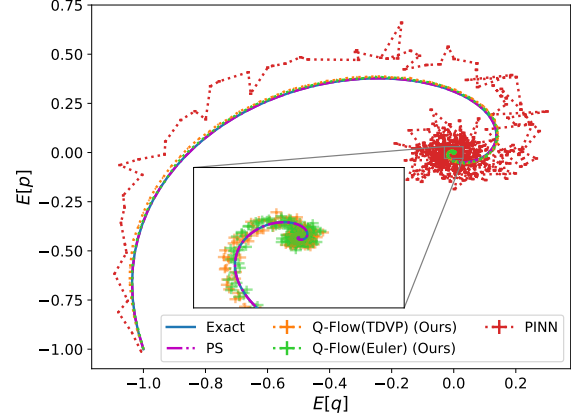


Figure 2. The trajectory of the centroids of the simulated distributions. The PINN baseline is excluded from the inset. Error bars are included for all except for the Exact and PS methods.

puts gives (Carmichael, 1999b)

$$\dot{Q} = \sum_j \left[\gamma_j + \frac{1}{4}\gamma_j(\bar{n}_j + 1) \left(\frac{\partial^2}{\partial q_j^2} + \frac{\partial^2}{\partial p_j^2} \right) + \left(\frac{\gamma_j}{2}q_j - \omega_j p_j \right) \frac{\partial}{\partial q_j} + \left(\frac{\gamma_j}{2}p_j + \omega_j q_j \right) \frac{\partial}{\partial p_j} \right] Q.$$

We test the simulation methods on three problems of increasing dimensionality: a 1-Well system, a 2-Well system, and a 20-Well system. For each system, we use a coherent state initial condition, which corresponds to a Gaussian with variance $1/2$. We center the Gaussian at $(-1, \dots, -1)$. As time passes this Gaussian spirals toward the origin and changes its standard deviation. To make the simulation more challenging, for every Well j we uniformly sample the system’s parameters $\bar{n}_j \in [3, 7)$, $\gamma_j \in [0.5, 1.5)$, and $\omega_j \in [0.5, 1.5)$.

Metrics. To evaluate a simulation method’s performance, we compute the L_1 Loss between each simulation and the exact distribution:

$$L_1[Q_{\text{sim}}, Q_{\text{exact}}] \equiv \int d^d x |Q_{\text{sim}}(x) - Q_{\text{exact}}(x)| \approx \frac{1}{N} \sum_{x \sim Q_{\text{exact}}} \left| \frac{Q_{\text{sim}}(x)}{Q_{\text{exact}}(x)} - 1 \right|. \quad (8)$$

Although the L_1 Loss is a useful metric, it is also illustrative to examine observables of the system. One observable is the centroid, $\mathbb{E}[\vec{x}] \approx \frac{1}{N} \sum_{x \sim Q_{\text{sim}}} \vec{x}$. With more Wells, we cannot easily plot the centroid trajectory, so instead we compute the centroid’s distance from the origin, $\|\mathbb{E}[\vec{x}]\|$.

Additionally, we compute a second observable, $\mathbb{E}[(\tilde{\mathcal{L}}Q/Q)^2]$, which we refer to as the *Liouvillian loss*. The Liouvillian loss measures the magnitude of the

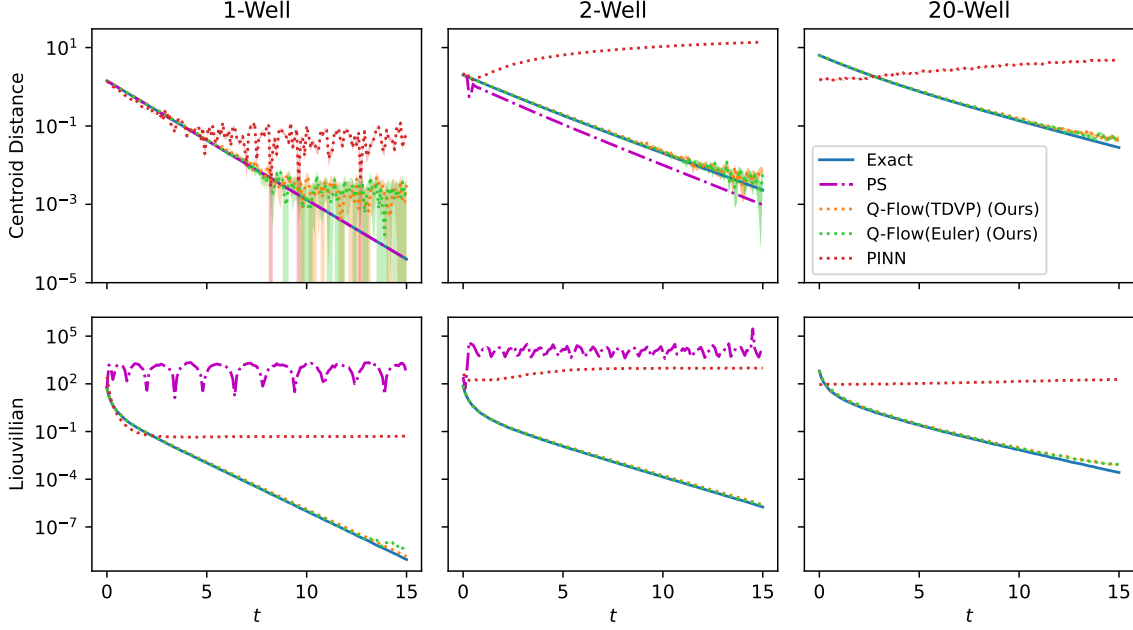


Figure 3. The simulated evolution of two observables for 1-Well, 2-Well, and 20-Well Fokker-Planck systems. Error bars are included for all except for the Exact and Pseudo-spectral results. The unit of time t is inversely proportional to the unit of γ_j .

dynamics relative to the distribution, an indicator of how perturbed the system is from equilibrium.

For the Euler and TDVP methods, we sample directly from the flow to compute expected values. For PINNs, we use Markov chain Monte Carlo (MCMC) to obtain samples. For pseudo-spectral results we compute expected values by summing over the grid and scaling by Q .

Results and Discussion. Table 1 shows the L_1 Loss between each simulation and the exact distribution for a number of simulation times. Although we do not include error bounds in the table for ease of viewing, the error is always at least an order of magnitude smaller than the value in question. The one exception is for the Pseudo-spectral method results, where because of our grid integration method, we do not compute error bounds. We also exclude the pseudo-spectral method from the 20-Well system because a grid size of only 10 would require at least 10^{40} values to be stored.

Both the Euler and TDVP methods have extremely low L_1 Loss. In fact, both methods perform better than the Pseudo-spectral method in the 2-Well case and in the later times of the 1-Well case. While increasing the number of Wells, we find that the Euler and TDVP methods continue to perform well while PINNs and pseudo-spectral methods struggle increasingly. Pseudo-spectral methods cannot simulate the 20-Well system due to the curse of dimensionality, and while PINNs can in principle simulate the system, in practice they perform extremely poorly. Indeed, the poor performance

of PINN is also related to the curse of dimensionality in sampling and optimization. This is because to train PINN, the standard practice is to randomly sample points or use the grid points from the problem domain, the complexity of which grows exponentially with the dimensionality. As a consequence, the loss and the gradients from finite samples are not accurate enough for PINN. In addition, PINN tries to learn the dynamics of multiple time steps simultaneously, which also increases the challenges to its representational ability. On the other hand, both the Euler and TDVP methods still consistently report low fidelities. Finally, note that the Euler method has a consistently lower L_1 loss than the TDVP method.

Figure 2 shows the trajectory of each simulation method’s centroid for the 1-Well case. Once again, the Euler and TDVP methods both closely match the exact evolution and the Euler method performs slightly better in general. On the other hand, the PINN solution exhibits consistently biased and rapidly fluctuating estimates of the centroid. As expected, the Pseudo-spectral method closely tracks the exact trajectory. However, we note that although our methods appear to match the exact results less accurately, the large error bars in the cutout demonstrate that this is in large part due to sampling error. We could have computed the centroid for the Euler and TDVP methods using grid integration as with the Pseudospectral method, but we instead choose to use sampling because this better generalizes to higher dimensions.

Figure 3 shows the evolution of the centroid distance and the Liouvillian Loss for all three problems. Euler and TDVP closely match the exact evolution of the two observables. Although the two methods’ estimates of the centroid distance begin to diverge from the exact centroid distance at around time 10, once again the large error bars demonstrate that this is due to error in the sampling estimate. Although the PINN centroid distance also begins to diverge from the desired value, the small error bars for this estimate suggest that the deviation does not come from sampling error.

In terms of the Liouvillian loss, both the Euler method and TDVP decrease consistently. At around time 15 the Euler Liouvillian loss jumps slightly, but this can most likely be improved by increasing the number of training steps per time step for the Euler method and by decreasing the learning rate. Further, this occurs at a Liouvillian loss of less than 10^{-7} , so the simulation is still likely precise enough for most applications. In practice, we find that decreasing the step size improves both the Euler and TDVP methods’ performance. Interestingly, the Pseudo-spectral method provides a very poor estimate of the Liouvillian loss. We suspect that this is due to error in numerical derivatives.

Finally, note that unlike the other methods, our methods continue to correctly simulate the system for large numbers of Wells. It is only toward the end of time evolution in the 20-Well case that our methods begin to show some deviation from the exact observables. Again, this can likely be reduced by decreasing the step size and taking more samples.

4.2. Dissipative Bosonic Model

Experimental Setup. The dissipative bosonic model is a frequently studied open quantum system (Kordas et al., 2013; Berg & Nyström, 2019). We test our methods on this model because it has a more complex evolution equation and because it has greater real-world applicability.

The dissipative bosonic model we use has (Kordas et al., 2013) $H = -J \sum_j (a_{j+1}^\dagger a_j + a_j^\dagger a_{j+1})$ and

$$\mathcal{L}_{\text{loss}} \rho = -\frac{1}{2} \sum_j \gamma_j (n_j \rho + \rho n_j - 2a_j \rho a_j^\dagger) \quad (9)$$

where $n_j = a_j^\dagger a_j$ and j enumerates the Wells. Converting to the Q function formalism gives that $\tilde{\mathcal{L}}$ is

$$\sum_j \gamma_j \left(\frac{1}{4} \left(\frac{\partial^2}{\partial q_j^2} + \frac{\partial^2}{\partial p_j^2} \right) + \frac{1}{2} \left(q_j \frac{\partial}{\partial q_j} + p_j \frac{\partial}{\partial p_j} + 1 \right) \right) + J \sum_j \left(p_{j+1} \frac{\partial}{\partial q_j} - q_{j+1} \frac{\partial}{\partial p_j} + p_j \frac{\partial}{\partial q_{j+1}} - q_j \frac{\partial}{\partial p_{j+1}} \right).$$

Following Figure 3 of (Kordas et al., 2015), we consider a 2-Well system with $J = 1$, $U = 0$, and $\gamma = [1, 0]$. We

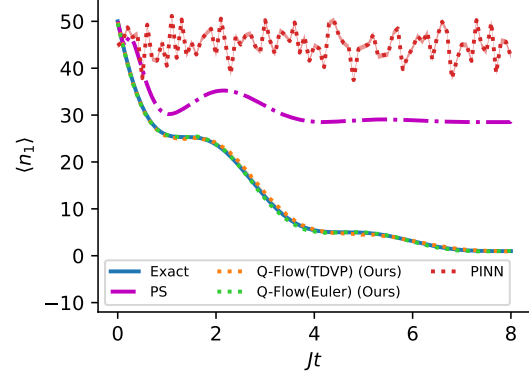


Figure 4. Dynamics of $\langle n_1 \rangle$ in a 2-Well dissipative bosonic model.

simulate the evolution of an antisymmetric Bose-Einstein Condensate (BEC) with 50 particles in each Well, which has a Q function $Q(q_1, p_1, q_2, p_2)$ given by

$$Q = \frac{[(q_1 - q_2)^2 + (p_1 - p_2)^2]^{100}}{\pi^2 \cdot 2^{100} \cdot 100!} e^{-(q_1^2 + p_1^2 + q_2^2 + p_2^2)}.$$

Because of the complex multimodal initial distribution, we use the Convex Potential Flow for these experiments. We pretrain the flow as described in Section 3.5.

Metric. For this system, we compute the observable $\langle n_1 \rangle \approx \frac{1}{N} \sum_{x \sim Q_{\text{sim}}} (q_1^2 + p_1^2 - 1)$ because it’s exact evolution is given in (Kordas et al., 2015).

Results and Discussion. We show the simulated evolution of $\langle n_1 \rangle$ in Figure 4. Both the Euler and TDVP methods closely match the exact evolution, demonstrating that our methods’ can handle multi-Well interactions correctly. In particular, the J term is responsible for the oscillations shown because it causes the two Wells to exchange particles.

5. Conclusion

In this work, we made a important contribution to the problem of simulating open quantum systems. We used a reformulation of the density matrix to the Husimi Q function, which allowed us to study open quantum systems as an evolution of a probability distribution under dynamics, described by a partial differential equation that we derive for each system. This allowed us to establish a direct connection between simulating continuous or bosonic open quantum systems and the rich literature on generative models in standard machine learning. With off-the-shelf normalizing flows, Affine Coupling Flows and Convex Potential Flows, and a new efficient method for solving high-dimensional PDEs, Euler-KL, we established Q-Flow, a new and efficient approach to simulation of open quantum systems.

We compared Q-Flow to the state-of-the-art numerical and

deep learning approaches on two important systems to the field, the dissipative harmonic oscillator and dissipative bosonic models. We established superior performance across the board, especially when the dimensionality of the system increases rapidly in an exponential manner.

We believe the significance of our results is twofold. On one hand, Q-Flow accurate simulation of open quantum systems can be further developed to aid progress in fundamental physics and engineering applications, such as superconductors and quantum computers. On the other hand, through our reformulation from evolving the density matrix to evolving the Q function, we shifted the modeling challenges from the curse of dimensionality to the accurate evolution of a high-dimensional deep generative model. Q-Flow can aid progress in evolving probability distributions under PDE dynamics and inspire future work on deep generative models.

6. Acknowledgement

The authors acknowledge helpful discussions with Zhuo Chen and Matija Medvidović. The authors acknowledge support from the NSF AI Institute for Artificial Intelligence and Fundamental Interactions (IAIFI). This material is based upon work supported by the U.S. Department of Energy, Office of Science, National Quantum Information Science Research Centers, Co-design Center for Quantum Advantage (C2QA) under contract number DE-SC0012704.

References

- Adesso, G., Ragy, S., and Lee, A. R. Continuous variable quantum information: Gaussian states and beyond. *Open Systems & Information Dynamics*, 21(01n02):1440001, 2014.
- Amari, S.-i. Neural learning in structured parameter spaces—natural riemannian gradient. *Advances in neural information processing systems*, 9, 1996.
- Amari, S.-I. Natural gradient works efficiently in learning. *Neural computation*, 10(2):251–276, 1998.
- Barreiro, J. T., Müller, M., Schindler, P., Nigg, D., Monz, T., Chwalla, M., Hennrich, M., Roos, C. F., Zoller, P., and Blatt, R. An open-system quantum simulator with trapped ions. *Nature*, 470(7335):486–491, 2011.
- Berg, J. and Nyström, K. Data-driven discovery of PDEs in complex datasets. *Journal of Computational Physics*, 384:239–252, 2019. ISSN 0021-9991. doi: <https://doi.org/10.1016/j.jcp.2019.01.036>. URL <http://www.sciencedirect.com/science/article/pii/S0021999119300944>.
- Bradbury, J., Frostig, R., Hawkins, P., Johnson, M. J., Leary, C., Maclaurin, D., Necula, G., Paszke, A., VanderPlas, J., Wanderman-Milne, S., and Zhang, Q. JAX: composable transformations of Python+NumPy programs, 2018. URL <http://github.com/google/jax>.
- Carleo, G. and Troyer, M. Solving the quantum many-body problem with artificial neural networks. *Science*, 355(6325):602–606, 2017. doi: 10.1126/science.aag2302.
- Carleo, G., Choo, K., Hofmann, D., Smith, J. E. T., Westerhout, T., Alet, F., Davis, E. J., Efthymiou, S., Glasser, I., Lin, S.-H., Mauri, M., Mazzola, G., Mendl, C. B., van Nieuwenburg, E., O’Reilly, O., Théveniaut, H., Torlai, G., Vicentini, F., and Wietek, A. Netket: A machine learning toolkit for many-body quantum systems. *SoftwareX*, pp. 100311, 2019. doi: 10.1016/j.softx.2019.100311. URL <http://www.sciencedirect.com/science/article/pii/S23527111019300974>.
- Carmichael, H. J. *Dissipation in Quantum Mechanics: The Master Equation Approach*, pp. 1–28. Springer Berlin Heidelberg, Berlin, Heidelberg, 1999a. ISBN 978-3-662-03875-8. doi: 10.1007/978-3-662-03875-8_1. URL https://doi.org/10.1007/978-3-662-03875-8_1.
- Carmichael, H. J. *Quantum—Classical Correspondence for the Electromagnetic Field II: P, Q, and Wigner Representations*, pp. 101–145. Springer Berlin Heidelberg, Berlin, Heidelberg, 1999b. ISBN 978-3-662-03875-8. doi: 10.1007/978-3-662-03875-8_4. URL https://doi.org/10.1007/978-3-662-03875-8_4.
- Cazalilla, M. A., Citro, R., Giamarchi, T., Orignac, E., and Rigol, M. One dimensional bosons: From condensed matter systems to ultracold gases. *Reviews of Modern Physics*, 83(4):1405, 2011.
- Chen, Z., Luo, D., Hu, K., and Clark, B. K. Simulating 2+ 1d lattice quantum electrodynamics at finite density with neural flow wavefunctions. *arXiv preprint arXiv:2212.06835*, 2022.
- Dinh, L., Krueger, D., and Bengio, Y. Nice: Non-linear independent components estimation. *arXiv preprint arXiv:1410.8516*, 2014.
- Dinh, L., Sohl-Dickstein, J., and Bengio, S. Density estimation using real NVP. In *International Conference on Learning Representations*, 2017. URL <https://openreview.net/forum?id=HkpbmH91x>.
- Fornberg, B. *A practical guide to pseudospectral methods*. Number 1. Cambridge university press, 1998.
- Grathwohl, W., Chen, R. T. Q., Bettencourt, J., and Duvenaud, D. Scalable reversible generative models with free-form continuous dynamics. In *International Conference on Learning Representations*, 2019. URL <https://openreview.net/forum?id=rJxgknCcK7>.

- Hartmann, M. J. and Carleo, G. Neural-network approach to dissipative quantum many-body dynamics. *Phys. Rev. Lett.*, 122:250502, Jun 2019. doi: 10.1103/PhysRevLett.122.250502. URL <https://link.aps.org/doi/10.1103/PhysRevLett.122.250502>.
- Hermann, J., Schätzle, Z., and Noé, F. Deep-neural-network solution of the electronic schrödinger equation. *Nature Chemistry*, 12(10):891–897, Oct 2020. ISSN 1755-4349. doi: 10.1038/s41557-020-0544-y.
- Huang, C.-W., Chen, R. T. Q., Tsirigotis, C., and Courville, A. Convex potential flows: Universal probability distributions with optimal transport and convex optimization. In *International Conference on Learning Representations*, 2021. URL <https://openreview.net/forum?id=te7PVH1sPxJ>.
- Häflner, D. and Vicentini, F. mpi4jax: Zero-copy mpi communication of jax arrays. *Journal of Open Source Software*, 6(65):3419, 2021. doi: 10.21105/joss.03419. URL <https://doi.org/10.21105/joss.03419>.
- Kordas, G., Wimberger, S., and Witthaut, D. Decay and fragmentation in an open bose-hubbard chain. *Phys. Rev. A*, 87:043618, Apr 2013. doi: 10.1103/PhysRevA.87.043618. URL <https://link.aps.org/doi/10.1103/PhysRevA.87.043618>.
- Kordas, G., Witthaut, D., Buonsante, P., Vezzani, A., Buri-
oni, R., Karanikas, A. I., and Wimberger, S. The dissipative Bose-Hubbard model. *European Physical Journal Special Topics*, 224(11):2127–2171, November 2015. doi: 10.1140/epjst/e2015-02528-2.
- Krishnapriyan, A., Gholami, A., Zhe, S., Kirby, R., and Mahoney, M. W. Characterizing possible failure modes in physics-informed neural networks. In Ranzato, M., Beygelzimer, A., Dauphin, Y., Liang, P., and Vaughan, J. W. (eds.), *Advances in Neural Information Processing Systems*, volume 34, pp. 26548–26560. Curran Associates, Inc., 2021. URL <https://proceedings.neurips.cc/paper/2021/file/df438e5206f31600e6ae4af72f2725f1-Paper.pdf>.
- Luo, D. and Clark, B. K. Backflow transformations via neural networks for quantum many-body wave functions. *Physical review letters*, 122(22):226401, 2019.
- Luo, D., Chen, Z., Hu, K., Zhao, Z., Hur, V. M., and Clark, B. K. Gauge invariant autoregressive neural networks for quantum lattice models. *arXiv preprint arXiv:2101.07243*, 2021.
- Luo, D., Chen, Z., Carrasquilla, J., and Clark, B. K. Autoregressive neural network for simulating open quantum systems via a probabilistic formulation. *Phys. Rev. Lett.*, 128:090501, Feb 2022a. doi: 10.1103/PhysRevLett.128.090501.
- Luo, D., Chen, Z., Carrasquilla, J., and Clark, B. K. Autoregressive neural network for simulating open quantum systems via a probabilistic formulation. *Physical review letters*, 128(9):090501, 2022b.
- Luo, D., Yuan, S., Stokes, J., and Clark, B. K. Gauge equivariant neural networks for 2+ 1d u(1) gauge theory simulations in hamiltonian formulation. *arXiv preprint arXiv:2211.03198*, 2022c.
- Martyn, J. M., Najafi, K., and Luo, D. Variational neural-network ansatz for continuum quantum field theory. *arXiv preprint arXiv:2212.00782*, 2022.
- McMillan, W. L. Ground state of liquid he 4. *Physical Review*, 138(2A):A442, 1965.
- Medvidović, M. and Sels, D. Towards unitary dynamics of large two-dimensional quantum rotor models. *arXiv preprint arXiv:2212.11289*, 2022.
- Nagy, A. and Savona, V. Variational quantum monte carlo method with a neural-network ansatz for open quantum systems. *Phys. Rev. Lett.*, 122:250501, Jun 2019. doi: 10.1103/PhysRevLett.122.250501. URL <https://link.aps.org/doi/10.1103/PhysRevLett.122.250501>.
- Paszke, A., Gross, S., Massa, F., Lerer, A., Bradbury, J., Chanan, G., Killeen, T., Lin, Z., Gimelshein, N., Antiga, L., et al. Pytorch: An imperative style, high-performance deep learning library. *Advances in neural information processing systems*, 32, 2019.
- Pescia, G., Han, J., Lovato, A., Lu, J., and Carleo, G. Neural-network quantum states for periodic systems in continuous space. *Physical Review Research*, 4(2):023138, 2022.
- Pfau, D., Spencer, J. S., Matthews, A. G. D. G., and Foulkes, W. M. C. Ab initio solution of the many-electron schrödinger equation with deep neural networks. *Phys. Rev. Res.*, 2:033429, Sep 2020. doi: 10.1103/PhysRevResearch.2.033429.
- Rackauckas, C. and Nie, Q. Differentialequations.jl—a performant and feature-rich ecosystem for solving differential equations in julia. *Journal of Open Research Software*, 5(1):15, 2017.
- Raissi, M. Deep hidden physics models: Deep learning of nonlinear partial differential equations. *Journal of Machine Learning Research*, 19(25):1–24, 2018. URL <http://jmlr.org/papers/v19/18-046.html>.

- Raissi, M., Perdikaris, P., and Karniadakis, G. Physics-informed neural networks: A deep learning framework for solving forward and inverse problems involving nonlinear partial differential equations. *Journal of Computational Physics*, 378:686–707, 2019. ISSN 0021-9991. doi: <https://doi.org/10.1016/j.jcp.2018.10.045>. URL <http://www.sciencedirect.com/science/article/pii/S0021999118307125>.
- Reh, M. and Gärttner, M. Variational monte carlo approach to partial differential equations with neural networks. *Machine Learning: Science and Technology*, 3(4):04LT02, 2022.
- Reh, M., Schmitt, M., and Gärttner, M. Time-dependent variational principle for open quantum systems with artificial neural networks. *Physical Review Letters*, 127(23):230501, 2021.
- Rezende, D. and Mohamed, S. Variational inference with normalizing flows. In *International conference on machine learning*, pp. 1530–1538. PMLR, 2015.
- Shankar, R. *Principles of quantum mechanics*. Springer Science & Business Media, 2012.
- Sharir, O., Levine, Y., Wies, N., Carleo, G., and Shashua, A. Deep autoregressive models for the efficient variational simulation of many-body quantum systems. *Phys. Rev. Lett.*, 124:020503, Jan 2020. doi: 10.1103/PhysRevLett.124.020503.
- Sorella, S. Green function monte carlo with stochastic reconfiguration. *Physical review letters*, 80(20):4558, 1998.
- Sorella, S. Generalized lanczos algorithm for variational quantum monte carlo. *Physical Review B*, 64(2):024512, 2001.
- Verstraete, F., Wolf, M. M., and Ignacio Cirac, J. Quantum computation and quantum-state engineering driven by dissipation. *Nature physics*, 5(9):633–636, 2009.
- Vicentini, F., Biella, A., Regnault, N., and Ciuti, C. Variational neural-network ansatz for steady states in open quantum systems. *Phys. Rev. Lett.*, 122:250503, Jun 2019. doi: 10.1103/PhysRevLett.122.250503. URL <https://link.aps.org/doi/10.1103/PhysRevLett.122.250503>.
- Vicentini, F., Hofmann, D., Szabó, A., Wu, D., Roth, C., Giuliani, C., Pescia, G., Nys, J., Vargas-Calderón, V., Astrakhansev, N., and Carleo, G. NetKet 3: Machine Learning Toolbox for Many-Body Quantum Systems. *SciPost Phys. Codebases*, pp. 7, 2022. doi: 10.21468/SciPostPhysCodeb.7. URL <https://scipost.org/10.21468/SciPostPhysCodeb.7>.
- Weinan, E., Han, J., and Jentzen, A. Algorithms for solving high dimensional pdes: from nonlinear monte carlo to machine learning. *Nonlinearity*, 35(1):278, 2021.
- Westerhout, T., Astrakhansev, N., Tikhonov, K. S., Katsnelson, M. I., and Bagrov, A. A. Generalization properties of neural network approximations to frustrated magnet ground states. *Nature communications*, 11(1):1593, 2020.
- Yoshioka, N. and Hamazaki, R. Constructing neural stationary states for open quantum many-body systems. *Phys. Rev. B*, 99:214306, Jun 2019. doi: 10.1103/PhysRevB.99.214306. URL <https://link.aps.org/doi/10.1103/PhysRevB.99.214306>.

A. Q Function Conversions

A.1. Quantum Preliminaries

Here, we provide a brief and intuitive introduction to the theory of bosonic systems. We intentionally simplify most of the definitions and focus on the important concepts to our study. For an in-depth discussion, please refer to (Shankar, 2012).

We will discuss a few important terms that we use throughout the main text.

Bracket notation. Such notation is used throughout the text to denote quantum states. Quantum states are elements of a complex vector space V , equipped with a Hermitian form. In our work we use the standard Hermitian inner product, which in math notation is $(\mathbf{v}, \mathbf{w}) = \mathbf{v}^\dagger \mathbf{w}$. Here \dagger denotes the complex conjugate, for any two vectors $\mathbf{v}, \mathbf{w} \in V$. In physics notation, we write \mathbf{v} as $|\mathbf{v}\rangle$ (known as a *ket*) and likewise for \mathbf{w} . We also use the notation $\langle \mathbf{v} | \equiv \mathbf{v}^\dagger$, and call this a *bra*. Then, $\mathbf{v}^\dagger \mathbf{w}$ can be written $\langle \mathbf{v} | \mathbf{w} \rangle$, or more concisely as $\langle \mathbf{v} | \mathbf{w} \rangle$. Furthermore, $|\mathbf{v}\rangle \langle \mathbf{w}|$ denotes the outer product of \mathbf{v} and \mathbf{w}^\dagger .

Vacuum states, the Fock space. In addition to using $|\cdot\rangle$ and $\langle \cdot|$ to denote arbitrary members of the Hilbert space and its dual. We also have special notation for a few members of the Hilbert space. It turns out that the Hilbert space for a single Well is spanned by a countably infinite set of basis vectors, which we label $|0\rangle, |1\rangle, \dots$. For multiple Wells, the total Hilbert space will be the tensor product of each particle's Hilbert space. To represent a general element of $|0\rangle, |1\rangle, \dots$, we will use a Roman letter inside the ket or bra.

Creation, annihilation operators and Coherent state. The creation operator a^\dagger satisfies $a^\dagger |n\rangle = \sqrt{n+1} |n+1\rangle$ and the annihilation operator a satisfies $a |n\rangle = \sqrt{n} |n-1\rangle$ with $a |0\rangle = 0$. The coherent state $|\alpha\rangle$ with a complex number α is defined as $|\alpha\rangle = e^{\alpha a^\dagger - \alpha^* a} |0\rangle$, where e should be interpreted as matrix exponential function.

Compute observables. In quantum mechanics, a density matrix ρ can be expressed as $\rho = \sum_{n,m} \rho_{n,m} |n\rangle \langle m|$ and an observable O can be expressed as $O = \sum_{n,m} O_{n,m} |n\rangle \langle m|$, where both ρ and O can be viewed as Hermitian matrices. It follows that the expectation value of the observable $\langle O \rangle = \text{tr}(\rho O) = \sum_{n,m} O_{n,m} \rho_{m,n}$.

A.2. Q Function to ρ

In this section, we show that for a given $Q(\alpha, \alpha^*)$, the density matrix ρ corresponding to it is given by

$$\langle m | \rho | n \rangle = \pi \sqrt{m!n!} \sum_{k=0}^{\min(m,n)} \frac{Q_{m-k,n-k}}{k!}, \quad (10)$$

where

$$Q_{a,b}(\alpha, \alpha^*) = \frac{1}{a!b!} \frac{\partial^{a+b}}{\partial^a \alpha \partial^b \alpha^*} Q(\alpha, \alpha^*) \Big|_{\alpha=\alpha^*=0}.$$

From expressing $\langle \alpha |$ and $|\alpha\rangle$ in terms of Harmonic Oscillator eigenstates, we have that

$$\begin{aligned} Q(\alpha, \alpha^*) &= \frac{1}{\pi} e^{-\alpha \alpha^*} \sum_{m=0}^{\infty} \sum_{n=0}^{\infty} \frac{\langle m | \rho | n \rangle}{\sqrt{m!n!}} \alpha^{*m} \alpha^n \\ &= \frac{1}{\pi} \left(\sum_{s=0}^{\infty} \frac{(-1)^s}{s!} (\alpha \alpha^*)^s \right) \sum_{m=0}^{\infty} \sum_{n=0}^{\infty} \frac{\langle m | \rho | n \rangle}{\sqrt{m!n!}} \alpha^{*m} \alpha^n \\ &= \frac{1}{\pi} \sum_{s=0}^{\infty} \sum_{m=0}^{\infty} \sum_{n=0}^{\infty} \frac{(-1)^s}{s!} \frac{\langle m | \rho | n \rangle}{\sqrt{m!n!}} (\alpha^*)^{m+s} \alpha^{n+s} \end{aligned}$$

To determine $\langle m | \rho | n \rangle$, we must thus invert this series. However, since we know the correct form, we can simply substitute

Equation 10 into the expression above and show that it correctly gives $Q(\alpha, \alpha^*)$:

$$\begin{aligned}
 & \frac{1}{\pi} \sum_{s=0}^{\infty} \sum_{m=0}^{\infty} \sum_{n=0}^{\infty} \frac{(-1)^s}{s!} \frac{\langle m | \rho | n \rangle}{\sqrt{m!n!}} (\alpha^*)^{m+s} \alpha^{n+s} \\
 &= \frac{1}{\pi} \sum_{s=0}^{\infty} \sum_{m=0}^{\infty} \sum_{n=0}^{\infty} \frac{(-1)^s}{s!} \frac{\pi \sqrt{m!n!} \sum_{k=0}^{\min(m,n)} \frac{Q_{m-k,n-k}}{k!}}{\sqrt{m!n!}} (\alpha^*)^{m+s} \alpha^{n+s} \\
 &= \sum_{s=0}^{\infty} \sum_{m=0}^{\infty} \sum_{n=0}^{\infty} \sum_{k=0}^{\min(m,n)} \frac{(-1)^s}{s!} \frac{Q_{m-k,n-k}}{k!} (\alpha^*)^{m+s} \alpha^{n+s}.
 \end{aligned}$$

Setting $a = m + s$ and $b = n + s$ gives

$$\sum_{a=0}^{\infty} \sum_{b=0}^{\infty} \sum_{s=0}^{\min(a,b)} \sum_{k=0}^{\min(a,b)-s} \frac{(-1)^s}{s!} \frac{Q_{a-k-s,b-k-s}}{k!} (\alpha^*)^a \alpha^b.$$

Then, setting $d = s + k$ gives

$$\begin{aligned}
 & \sum_{a=0}^{\infty} \sum_{b=0}^{\infty} \sum_{d=0}^{\min(a,b)} \sum_{s=0}^d \frac{(-1)^s}{s!} \frac{Q_{a-d,b-d}}{(d-s)!} (\alpha^*)^a \alpha^b \\
 &= \sum_{a=0}^{\infty} \sum_{b=0}^{\infty} (\alpha^*)^a \alpha^b \sum_{d=0}^{\min(a,b)} Q_{a-d,b-d} \sum_{s=0}^d (-1)^s \binom{d}{s}.
 \end{aligned}$$

Now, by the Binomial Theorem, $\sum_{s=0}^d (-1)^s \binom{d}{s} = (1-1)^d = 0^d$, which is 0 unless $d = 1$. So, we get

$$\begin{aligned}
 & \sum_{a=0}^{\infty} \sum_{b=0}^{\infty} Q_{a,b}(\alpha, \alpha^*) \cdot (\alpha^*)^a \alpha^b \\
 &= \sum_{a=0}^{\infty} \sum_{b=0}^{\infty} \frac{(\alpha^*)^a \alpha^b}{a!b!} \frac{\partial^{a+b}}{\partial^a \alpha \partial^b \alpha^*} Q(\alpha, \alpha^*) \\
 &= Q(\alpha, \alpha^*),
 \end{aligned}$$

as desired. The last step comes from the Taylor series representation of Q , which is only valid if Q is analytic. So as long as Q is analytic, this result holds.

Example. To convert a Liouvillian to an equation of motion for Q , we use the fact that

$$\dot{\rho} = (a^\dagger)^j a^k \rho (a^\dagger)^l a^m, \tag{11}$$

corresponds to

$$\dot{Q} = (\alpha^*)^j \left(\alpha + \frac{\partial}{\partial \alpha^*} \right)^k \alpha^m \left(\alpha^* + \frac{\partial}{\partial \alpha} \right)^l Q. \tag{12}$$

A linear combination of terms of the form in Equation 11 corresponds to the same linear combination of the corresponding terms in Equation 12.

A.3. Coherent State Identities

$$\begin{aligned}
 a^\dagger |\alpha\rangle &= a^\dagger e^{-|\alpha|^2/2} \sum_{n=0}^{\infty} \frac{\alpha^n}{\sqrt{n!}} |n\rangle \\
 &= e^{-|\alpha|^2/2} \sum_{n=0}^{\infty} \frac{\alpha^n}{\sqrt{n!}} \sqrt{n+1} |n+1\rangle \\
 &= e^{-|\alpha|^2/2} \frac{\partial}{\partial \alpha} \sum_{n=0}^{\infty} \frac{\alpha^{n+1}}{\sqrt{(n+1)!}} |n+1\rangle \\
 &= e^{-|\alpha|^2/2} \frac{\partial}{\partial \alpha} \sum_{n=0}^{\infty} \frac{\alpha^n}{\sqrt{n!}} |n\rangle \\
 &= e^{-|\alpha|^2/2} \frac{\partial}{\partial \alpha} \sum_{n=0}^{\infty} \frac{\alpha^n}{\sqrt{n!}} |n\rangle \\
 &= \frac{\partial}{\partial \alpha} e^{-|\alpha|^2/2} \sum_{n=0}^{\infty} \frac{\alpha^n}{\sqrt{n!}} |n\rangle - \left(\frac{\partial}{\partial \alpha} e^{-|\alpha|^2/2} \right) \sum_{n=0}^{\infty} \frac{\alpha^n}{\sqrt{n!}} |n\rangle \\
 &= \frac{\partial}{\partial \alpha} e^{-|\alpha|^2/2} \sum_{n=0}^{\infty} \frac{\alpha^n}{\sqrt{n!}} |n\rangle - \left(\frac{\partial}{\partial \alpha} e^{-|\alpha|^2/2} \right) \sum_{n=0}^{\infty} \frac{\alpha^n}{\sqrt{n!}} |n\rangle \\
 &= \frac{\partial}{\partial \alpha} e^{-|\alpha|^2/2} \sum_{n=0}^{\infty} \frac{\alpha^n}{\sqrt{n!}} |n\rangle + \frac{\alpha^*}{2} e^{-|\alpha|^2/2} \sum_{n=0}^{\infty} \frac{\alpha^n}{\sqrt{n!}} |n\rangle \\
 &= \left(\frac{\alpha^*}{2} + \frac{\partial}{\partial \alpha} \right) e^{-|\alpha|^2/2} \sum_{n=0}^{\infty} \frac{\alpha^n}{\sqrt{n!}} |n\rangle \\
 &= \left(\frac{\alpha^*}{2} + \frac{\partial}{\partial \alpha} \right) |\alpha\rangle.
 \end{aligned}$$

Similarly,

$$\langle \alpha | a = \left(\frac{\alpha}{2} + \frac{\partial}{\partial \alpha^*} \right) \langle \alpha |.$$

Also,

$$\frac{\partial}{\partial \alpha^*} |\alpha\rangle = \frac{\partial}{\partial \alpha^*} e^{-|\alpha|^2/2} \sum_{n=0}^{\infty} \frac{\alpha^n}{\sqrt{n!}} |n\rangle = -\frac{\alpha}{2} e^{-|\alpha|^2/2} \sum_{n=0}^{\infty} \frac{\alpha^n}{\sqrt{n!}} |n\rangle = -\frac{\alpha}{2} |\alpha\rangle \quad (13)$$

and

$$\frac{\partial}{\partial \alpha} \langle \alpha | = -\frac{\alpha^*}{2} \langle \alpha |.$$

A.4. ρ Evolution to Q Function Evolution

Note that

$$\begin{aligned}
 \langle \alpha | a^\dagger \hat{O}_1 \rho \hat{O}_2 | \alpha \rangle &= \alpha^* \langle \alpha | \hat{O}_1 \rho \hat{O}_2 | \alpha \rangle, \\
 \langle \alpha | \hat{O}_1 \rho \hat{O}_2 a | \alpha \rangle &= \alpha \langle \alpha | \hat{O}_1 \rho \hat{O}_2 | \alpha \rangle.
 \end{aligned}$$

Also,

$$\begin{aligned}
 \langle \alpha | a \hat{O}_1 \rho \hat{O}_2 | \alpha \rangle &= \left[\left(\frac{\alpha}{2} + \frac{\partial}{\partial \alpha^*} \right) \langle \alpha | \right] \hat{O}_1 \rho \hat{O}_2 | \alpha \rangle \\
 &= \left(\frac{\alpha}{2} + \frac{\partial}{\partial \alpha^*} \right) \langle \alpha | \hat{O}_1 \rho \hat{O}_2 | \alpha \rangle - \langle \alpha | \hat{O}_1 \rho \hat{O}_2 \frac{\partial}{\partial \alpha^*} | \alpha \rangle \\
 &= \left(\frac{\alpha}{2} + \frac{\partial}{\partial \alpha^*} \right) \langle \alpha | \hat{O}_1 \rho \hat{O}_2 | \alpha \rangle + \frac{\alpha}{2} \langle \alpha | \hat{O}_1 \rho \hat{O}_2 | \alpha \rangle \\
 &= \left(\alpha + \frac{\partial}{\partial \alpha^*} \right) \langle \alpha | \hat{O}_1 \rho \hat{O}_2 | \alpha \rangle,
 \end{aligned}$$

and

$$\begin{aligned}
 \langle \alpha | \hat{O}_1 \rho \hat{O}_2 a^\dagger | \alpha \rangle &= \langle \alpha | \hat{O}_1 \rho \hat{O}_2 \left(\frac{\alpha^*}{2} + \frac{\partial}{\partial \alpha} \right) | \alpha \rangle \\
 &= \left(\frac{\alpha^*}{2} + \frac{\partial}{\partial \alpha} \right) \langle \alpha | \hat{O}_1 \rho \hat{O}_2 | \alpha \rangle - \left[\frac{\partial}{\partial \alpha} \langle \alpha | \right] \hat{O}_1 \rho \hat{O}_2 | \alpha \rangle \\
 &= \left(\frac{\alpha^*}{2} + \frac{\partial}{\partial \alpha} \right) \langle \alpha | \hat{O}_1 \rho \hat{O}_2 | \alpha \rangle + \frac{\alpha^*}{2} \langle \alpha | \hat{O}_1 \rho \hat{O}_2 | \alpha \rangle \\
 &= \left(\alpha^* + \frac{\partial}{\partial \alpha} \right) \langle \alpha | \hat{O}_1 \rho \hat{O}_2 | \alpha \rangle.
 \end{aligned}$$

With these results, we now have that for an equation of the form

$$\dot{\rho} = \sum_{j,k,l,m} c_{j,k,l,m} (a^\dagger)^j a^k \rho (a^\dagger)^l a^m,$$

we can convert the the Q function equation of motion by inserting $\frac{1}{\pi} \langle \alpha | \cdot | \alpha \rangle$ to get

$$\begin{aligned}
 \frac{1}{\pi} \langle \alpha | \dot{\rho} | \alpha \rangle &= \frac{1}{\pi} \sum_{j,k,l,m} c_{j,k,l,m} \langle \alpha | (a^\dagger)^j a^k \rho (a^\dagger)^l a^m | \alpha \rangle \\
 \implies \dot{Q}(\alpha, \alpha^*) &= \frac{1}{\pi} \sum_{j,k,l,m} c_{j,k,l,m} (\alpha^*)^j \langle \alpha | a^k \rho (a^\dagger)^l a^m | \alpha \rangle \\
 \implies \dot{Q}(\alpha, \alpha^*) &= \frac{1}{\pi} \sum_{j,k,l,m} c_{j,k,l,m} (\alpha^*)^j \left(\alpha + \frac{\partial}{\partial \alpha^*} \right)^k \langle \alpha | \rho (a^\dagger)^l a^m | \alpha \rangle \\
 \implies \dot{Q}(\alpha, \alpha^*) &= \frac{1}{\pi} \sum_{j,k,l,m} c_{j,k,l,m} (\alpha^*)^j \left(\alpha + \frac{\partial}{\partial \alpha^*} \right)^k \alpha^m \langle \alpha | \rho (a^\dagger)^l | \alpha \rangle \\
 \implies \dot{Q}(\alpha, \alpha^*) &= \frac{1}{\pi} \sum_{j,k,l,m} c_{j,k,l,m} (\alpha^*)^j \left(\alpha + \frac{\partial}{\partial \alpha^*} \right)^k \alpha^m \left(\alpha^* + \frac{\partial}{\partial \alpha} \right)^l \langle \alpha | \rho | \alpha \rangle \\
 \implies \dot{Q}(\alpha, \alpha^*) &= \sum_{j,k,l,m} c_{j,k,l,m} (\alpha^*)^j \left(\alpha + \frac{\partial}{\partial \alpha^*} \right)^k \alpha^m \left(\alpha^* + \frac{\partial}{\partial \alpha} \right)^l Q(\alpha, \alpha^*).
 \end{aligned}$$

A.5. Observable calculation with respect to Q function

Consider a general observable \hat{O} . Its expected value given a density matrix ρ is

$$\langle \hat{O} \rangle = \text{Tr}(\hat{O} \rho). \tag{14}$$

Inserting the coherent state resolution of the identity, we get that

$$\begin{aligned}\text{Tr}(\hat{O}\rho) &= \int \frac{d\alpha d\alpha^*}{\pi} \text{Tr}(\hat{O}\rho|\alpha\rangle\langle\alpha|) \\ &= \int \frac{d\alpha d\alpha^*}{\pi} \langle\alpha|\hat{O}\rho|\alpha\rangle.\end{aligned}$$

Depending on the operator, it may be most useful to insert the resolution of the identity elsewhere.

Example The expected value of $a^m(a^\dagger)^n$ given a density matrix ρ is

$$\begin{aligned}\langle a^m (a^\dagger)^n \rangle &= \text{Tr} \left(a^m (a^\dagger)^n \rho \right) \\ &= \int \frac{d\alpha d\alpha^*}{\pi} \text{Tr} \left(a^m |\alpha\rangle\langle\alpha| (a^\dagger)^n \rho \right) \\ &= \int \frac{d\alpha d\alpha^*}{\pi} \langle\alpha| (a^\dagger)^n \rho a^m |\alpha\rangle \\ &= \int \frac{d\alpha d\alpha^*}{\pi} \alpha^m (\alpha^*)^n \langle\alpha|\rho|\alpha\rangle \\ &= \int dq dp (q + ip)^m (q - ip)^n Q(q, p).\end{aligned}$$

If $m \neq n$, this is not an observable, but could be made an observable by adding its Hermitian conjugate.

B. Stochastic Euler-KL Method

Here we derive Equation 5 for the control-variance gradient of the KL-Divergence. We start with

$$KL(Q_\theta^{t+dt} || Q_\mathcal{L}^t) = \int Q_\theta^{t+dt} \ln \frac{Q_\theta^{t+dt}}{Q_\mathcal{L}^t}.$$

Taking the gradient gives

$$\begin{aligned}\nabla_\theta KL(Q_\theta^{t+dt} || Q_\mathcal{L}^t) &= \nabla_\theta \int Q_\theta^{t+dt} \ln \frac{Q_\theta^{t+dt}}{Q_\mathcal{L}^t} \\ &= \int (\nabla_\theta Q_\theta^{t+dt}) \ln \frac{Q_\theta^{t+dt}}{Q_\mathcal{L}^t} + \int Q_\theta^{t+dt} \nabla_\theta \ln \frac{Q_\theta^{t+dt}}{Q_\mathcal{L}^t} \\ &= \int Q_\theta^{t+dt} (\nabla_\theta \ln Q_\theta^{t+dt}) \ln \frac{Q_\theta^{t+dt}}{Q_\mathcal{L}^t} + \int Q_\theta^{t+dt} \nabla_\theta \ln Q_\theta^{t+dt} \\ &= \int Q_\theta^{t+dt} \left[\ln \frac{Q_\theta^{t+dt}}{Q_\mathcal{L}^t} + 1 \right] \nabla_\theta \ln Q_\theta^{t+dt}.\end{aligned}$$

Now, note that

$$\int Q_\theta^{t+dt}(x) \nabla_\theta \ln Q_\theta^{t+dt}(x) = \int Q_\theta^{t+dt}(x) \frac{\nabla_\theta Q_\theta^{t+dt}(x)}{Q_\theta^{t+dt}(x)} = \int \nabla_\theta Q_\theta^{t+dt}(x) = \nabla_\theta \int Q_\theta^{t+dt}(x) = \nabla_\theta 1 = 0. \quad (15)$$

So, letting

$$b = \int Q_\theta^{t+dt} \ln \frac{Q_\theta^{t+dt}(x)}{Q_\mathcal{L}^t(x)} \approx \frac{1}{N} \sum_{x \sim Q_\theta^{t+dt}} \ln \frac{Q_\theta^{t+dt}(x)}{Q_\mathcal{L}^t(x)}, \quad (16)$$

we can subtract a control variance to get

$$\begin{aligned}
 \nabla_{\theta} KL(Q_{\theta}^{t+dt} || Q_{\mathcal{L}}^t) &= \int Q_{\theta}^{t+dt} \left[\ln \frac{Q_{\theta}^{t+dt}}{Q_{\mathcal{L}}^t} + 1 \right] \nabla_{\theta} \ln Q_{\theta}^{t+dt} \\
 &= \int Q_{\theta}^{t+dt} \left[\ln \frac{Q_{\theta}^{t+dt}}{Q_{\mathcal{L}}^t} + 1 \right] \nabla_{\theta} \ln Q_{\theta}^{t+dt} - (b+1) \int Q_{\theta}^{t+dt}(x) \nabla_{\theta} \ln Q_{\theta}^{t+dt}(x) \\
 &= \int Q_{\theta}^{t+dt} \left[\ln \frac{Q_{\theta}^{t+dt}}{Q_{\mathcal{L}}^t} - b \right] \nabla_{\theta} \ln Q_{\theta}^{t+dt} \\
 &= \int Q_{\theta}^{t+dt} \left[\ln \frac{Q_{\theta}^{t+dt}}{Q_{\mathcal{L}}^t} - b \right] \nabla_{\theta} \ln Q_{\theta}^{t+dt}
 \end{aligned}$$

Finally, approximating the integral gives

$$\begin{aligned}
 \nabla_{\theta} KL(Q_{\theta}^{t+dt} || Q_{\mathcal{L}}^t) &= \int Q_{\theta}^{t+dt} \left[\ln \frac{Q_{\theta}^{t+dt}}{Q_{\mathcal{L}}^t} - b \right] \nabla_{\theta} \ln Q_{\theta}^{t+dt} \\
 &\approx \frac{1}{N} \sum_{x \sim Q_{\theta}^{t+dt}} \left[\ln \frac{Q_{\theta}^{t+dt}}{Q_{\mathcal{L}}^t} - b \right] \nabla_{\theta} \ln Q_{\theta}^{t+dt},
 \end{aligned}$$

as desired.

C. Additional Experimental Details

C.1. Pseudo-spectral baseline details

As a baseline approach to solving the Q function evolution PDE (Eq. 2), we implement a pseudo-spectral discretization of the PDE (Fornberg, 1998) in a square domain with $-10 < q_j < 10$ and $-10 < p_j < 10$ for each Well j , set $Q = 0$ at the boundaries, and integrate using an adaptive Tsitouras 5/4 Runge-Kutta solver (Tsit5) (Rackauckas & Nie, 2017) while projecting at each time step to ensure the probability density Q remains positive and normalized. We use a grid size of 256 grid points per dimension for 1-Well and 32 grid points per dimension for 2-Wells, resulting in a state size of $256^2 = 65,536$ for 1-Well and $32^4 = 1,048,576$ for 2-Wells. Note that for a fixed grid size, the state grows exponentially with the number of Wells—i.e. the curse of dimensionality. This limits our ability to perform more fine-grained simulations on larger domains and makes this baseline approach intractable for more than a few Wells.

C.2. PINN baseline details

We also use Physics Informed Neural Networks (PINNs) as a baseline. To implement this, we use the PINA library which is built on top of PyTorch. For each problem, we have two loss terms. The first computes the L_2 loss between the predicted initial distribution and the actual initial distribution for points sampled uniformly from within the domain of the solver at $t = 0$. The second computes the L_2 loss between the PINN time derivative and the predicted time derivative $\tilde{\mathcal{L}}Q$ at points sampled uniformly from within the spacial and temporal domain of the solver. The total loss is the sum of these two losses. We then optimize using gradient decent. Every 500 epochs we re-sample the points with which to compute the loss. For each experiment, we use a fully connected network with skip connections. The layer sizes are [input size, 40, 40, 40, 1]. The following are the hyperparameters used for each of the experiments:

- **1-Well Harmonic Oscillator:** We use 1000 samples at a time for the initial condition and 50000 samples at a time for the derivative condition. We train for 25000 epochs with a learning rate of 0.001.
- **2-Well Harmonic Oscillator:** We use 1000 samples at a time for the initial condition and 30000 samples at a time for the derivative condition. We train for 25000 epochs with a learning rate of 0.001.

- **20-Well Harmonic Oscillator:** We use 3000 samples at a time for the initial condition and 3000 samples at a time for the derivative condition. We train for 50000 epochs with a learning rate of 0.001. Here, we have to decrease the number of samples for the derivative condition because of memory limits.
- **2-Well Dissipative Bosonic Model:** We use 1000 samples at a time for the initial condition and 30000 samples at a time for the derivative condition. We train for 25000 epochs with a learning rate of 0.001.

C.3. Euler experiment details

Below are the hyperparameters we use for the Euler method. For the Harmonic Oscillator results we use a 3 layer RealNVP where each affine transformation is a 2 hidden layer feed forward neural network with hidden layers of size 5. For the Dissipative Bosonic Model result, we use a Convex Potential Flow with a 5 hidden layer input-convex neural network with hidden layers of size 20 and augmented layers of size 4, see (Huang et al., 2021).

- **1-Well Harmonic Oscillator:** We train for 1500 steps with a step size of 0.01. For each step, we use the KL control variance loss to fit for 150 epochs with a learning rate of 0.001. We use 1000 samples per fitting epoch.
- **2-Well Harmonic Oscillator:** We train for 1500 steps with a step size of 0.01. For each step, we use the KL control variance loss to fit for 150 epochs with a learning rate of 0.001. We use 1000 samples per fitting epoch.
- **20-Well Harmonic Oscillator:** We train for 1500 steps with a step size of 0.01. For each step, we use the KL control variance loss to fit for 150 epochs with a learning rate of 0.001. We use 10000 samples per fitting epoch.
- **2-Well Dissipative Bosonic Model:** We train for 400 steps with a step size of 0.02. For each step, we use the KL control variance loss to fit for 200 epochs with a learning rate of 0.002. We use 10000 samples per fitting epoch.

C.4. TDVP experiment details

Below are the hyperparameters we use for the TDVP method. For the Harmonic Oscillator results we use a 3 layer RealNVP where each affine transformation is a 2 hidden layer feed forward neural network with hidden layers of size 5. For the Dissipative Bosonic Model result, we use a Convex Potential Flow with a 5 hidden layer input-convex neural network with hidden layers of size 20 and augmented layers of size 4, see (Huang et al., 2021).

- **1-Well Harmonic Oscillator:** We train for 1500 steps with a step size of 0.01. We use 1000 samples per step. We use a diagonal shift of 0.01.
- **2-Well Harmonic Oscillator:** We train for 1500 steps with a step size of 0.01. We use 1000 samples per step. We use a diagonal shift of 0.01.
- **20-Well Harmonic Oscillator:** We train for 1500 steps with a step size of 0.01. We use 10000 samples per step. We use a diagonal shift of 0.01.
- **2-Well Dissipative Bosonic Model:** We train for 2000 steps with a step size of 0.004. We use 10000 samples per step. We use a diagonal shift of 0.01.